Additive Manufacturing of Transparent Glass Structures

3D PRINTING AND ADDITIVE MANUFACTURING
Volume 5, Number 4, 2018

DOI: 10.1089/3dp.2018.0157

ORIGINAL ARTICLE

Additive Manufacturing of Transparent Glass Structures

Chikara Inamura,[1,*] Michael Stern,[1,*] Daniel Lizardo,[1,*] Peter Houk,[2] and Neri Oxman[1]

Abstract

Advancements in manufacturing during the Industrial Revolution enabled the widespread use of glass in buildings and household objects. Nonetheless, processes for the fabrication of complex geometry and custom objects with glass remain elusive. We present G3DP2—a second iteration of the novel additive manufacturing (AM) technology for transparent glass products developed by The Mediated Matter Group at MIT. One of the oldest production materials, glass involves complex material chemistry and requires extreme working temperatures underlying the persistent challenges associated with its design and production. AM with molten glass presents a potential path toward production of highly complex geometry and custom-designed objects while retaining the optical transparency and chemical stability available through traditional manufacturing processes. G3DP2 is a new AM platform for molten glass that combines digitally integrated three-zone thermal control system with four-axis motion control system, introducing industrial-scale production capabilities with enhanced production rate and reliability while ensuring product accuracy and repeatability, all previously unattainable for glass. A series of material characterizations were conducted to evaluate the mechanical properties of the 3D-printed glass products produced by G3DP2. A set of 3-m-tall glass columns was designed, engineered, and digitally fabricated for Milan Design Week 2017, highlighting the geometric complexity, accuracy, strength, and transparency of 3D-printed glass at an architectural scale for the first time and a critical step in utilizing the true structural capacity of the material. Together, the installation and the G3DP2 platform serve as a foundation for future work and suggest exciting possibilities associated with the digital fabrication of glass as well as potential applications in product and architectural design.

Keywords: 3D printing, additive manufacturing, glass, glass structures, printed glass, transparent

Introduction

Glass and the built environment

Glass is one of the oldest production materials. Its earliest appearance as cast glass during 2500 BCE and blown glass in 100 BCE has changed little throughout history constrained by the complex material chemistry and extreme working temperatures required. Innovations in glass blowing and molding, combined with seminal glass science research, revolutionized glass making and enabled individual production lines to output ~10 million containers per year or 2000 light bulbs per minute.[1] During the same period, the invention of the float glass manufacturing process allowed for faster continuous production of flat glass panels.[2] The rate of flat glass production increased by 25 times, a sixfold increase per capita, between 1899 and 2009,[3–5] and industrialization brought a new wave of affordable glass products with increased performance (see Supplementary Data; Supplementary Data are available online at www.liebertpub.com/3dp). Machine-made bottles, light bulbs, and windows have all contributed to reshaping the world and the built environment. Alas, these products were characterized by increased homogeneity and decreased customizability.

Since the mid-20th century, glass manufacturing has shifted again, with a diverse group of functionalized products arising from innovations in glass chemistry, including chemical doping for high-strength sheet glass and controlled refractive index for fiber optic data lines. These processes have expanded the applications of glass products, but geometries remain simple as the cost of complexity remains prohibitively high. Recent studies on additive manufacturing (AM) of glass suggest possible intersections of both types of

[1]The Mediated Matter Group, MIT Media Lab, Massachusetts Institute of Technology, Cambridge, Massachusetts.
[2]MIT Glass Lab, Massachusetts Institute of Technology, Cambridge, Massachusetts.
*These authors contributed equally to this work.

Opposite page: 3D printed glass column installation. Milan Design Week 2017. *Photo Credit:* Paula Aguilera and Jonathan Williams.

sectors, where creativity and complexity are achieved without limitation by quality, performance, or cost.

Glass in architecture

Although glass windows existed in Rome by 100 ACE,[6] early architectural windows predominantly comprised of other translucent materials, including shells, minerals, and hide. Even as late as the Middle Ages, stained glass adorned only the most ornate structures.[7] Glass making technologies and applications of glass products evolved throughout the Modern Era, and by the turn of 19th century, glass had begun to appear in substantial parts of the built environment.

As of 2015, the global market for glass production was >200 million tons. Of that, the building sector uses 59 million tons $\sim$7.3 billion square meters of plate glass, embracing the low cost and ubiquity of the current industry to populate skylines and allow daylight into homes. Economically, the architectural glass represents a $\sim$45-billion-dollar industry.[8]

Printed glass

AM was invented over 30 years ago, but only in the last decade has it spread from rapid prototyping to rapid manufacturing (RM), which is defined as the industrial application of AM to produce functional end-use parts rather than prototypes. This shift was driven by a collective effort across disciplines, from engineers and scientists developing improved machines and materials to designers and artists acquiring advanced knowledge and implementing novel applications, such that today, RM accounts for at least 60% of all printed parts. The economic impact of RM is magnified by continued industrial growth, at an average growth rate of 25.9% over the last 28 years.[9]

Early examples of 3D printing with sintered glass powder lack the transparency and mechanical properties that the material is prized for, but represent serious attempts to industrialize a glass manufacturing process with complex geometry at reduced cost.[10,11] In recent years, new methods for printing glass have emerged, and dramatically changed the potential of AM for glass designs and products by enabling the creation of objects with increased geometric complexity, optical transparency, and reliability of mechanical strength.

Several major developments in high-resolution sintered glass printing have been achieved through vat photopolymerization and direct ink writing, in which silicate glass particles are suspended in resin and formed into complex geometries.[12,13]Postprocessing is then required to remove the resin and generate a glass body. As an example in the Kotz *et al.* process, the resin–glass composite forms undergo a 50-h debinding and vacuum furnace treatment at 1300°C and 0.005 millibar to remove trapped air and heal cracks. This approach is suitable for fabricating small and highly detailed parts such as microfluidics and optics because it delivers high precision and optical transparency. However, dependency on typical high-resolution vat photopolymerization systems limits the speed of this process to print glass at a rate of $\sim$0.02 kg/h (see Supplementary Data).[12,14,15] An additional challenge in scaling this indirect methodology is the high level of shrinkage and distortion which occurs as the binder is removed during the sintering process.

Recent advancements in glass printing technology also include nonsintered processes such as material extrusions with both solid and molten feedstock. Similar to traditional plastic fused deposition modeling, a stick-based material feedstock and high-temperature nozzle process was developed by Micron3DP as a means to print detailed glass objects with fine layer thickness. Little technical information has been published, but this similarity to plastic systems suggests a print rate of $\sim$0.05 kg/h (see Supplementary Data).[16] One of the limitations of the use of small filament size is that light scatters as it passes through the printed walls of the object, rendering it more translucent than transparent.[17,18] Alternately, a method for extruding much larger filaments that achieve transparency by using molten material stock extruded through a heated nozzle was developed by the Mediated Matter Group at MIT in 2014 and reported in 2015, and is noted hereafter as G3DP.[19] The first version of this process had a typical deposition rate of 2.2 kg/h (see Supplementary Data) and build chamber dimensions of $250 \times 250 \times 300$ mm, making it 42 times faster than Micron3DP and 118 times faster than a typical high-resolution vat photopolymerization while also achieving optical transparency.[20]

Goals for the industrial-scale glass 3D printer G3DP2

The first phase of glass printer development focused on a proof of concept that demonstrated the feasibility of creating optically transparent objects through the deposition of molten glass. The second phase focused on research and development of an industrial-scale platform, and established a new set of objectives that guided system design, development, and production of parts. With structural applications the goal, dimensional accuracy, and fidelity of both process and product were the measures of feasibility, linking two distinct objectives, which were pursued together. These objectives served as a backbone for the research presented in this article and are summarized here:

1. Develop an industrial-scale molten glass feedstock 3D printer by extending the research previously conducted at MIT, enhancing the material properties and range of products that could be produced.
2. Develop an architectural-scale 3D-printed glass structure to evaluate the practical capabilities of the new system in an industrial production.

New Platform: From Prototype to Industrial Platform

System architecture

Key performance metrics of speed, volume, repeatability, and reliability were identified for improvement in upgrading the platform for industrial and architectural output capability. In addition, the small feed volume and fragility of components in the previous platform (including a mobile ceramic print head and resistive heater) challenged the scale of output. Improving it required addressing even greater physical and thermal inertia and stress on mechanical components, prompting a ground-up machine redesign. The new platform is a two-part vertical assembly: an upper, stationary thermal module with a digitally integrated three-zone heating control system regulating glass flow and a lower, motion module with a four-axis computer numerical control (CNC) system that moves the print bed.

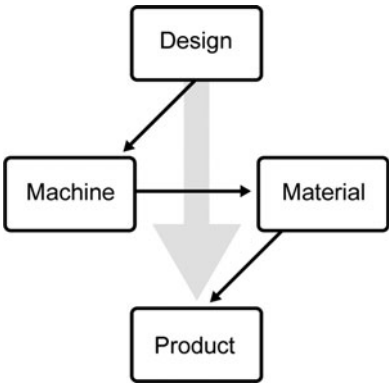

FIG. 1. A flowchart diagram illustrating the printing process and its confounding sensitivity to both the machine and material behaviors.

In this architecture, the thermal energy applied to the heating system was decoupled from the mechanical load of the motion system. This allowed for improved durability of both systems through careful consideration of material properties and detailed analysis of constituent parts supporting each separate module. Still, critical focus was given to the print head itself, situated at the interface between the modules and requiring the highest thermal and mechanical performance from its material choice.

Printed glass behavior: understanding and control

A critical challenge in developing industrial glass manufacturing is to understand material behavior across a wide range of temperatures. Glass is a viscous liquid with many nonlinear properties, and its behavior is highly sensitive to temperature. Furthermore, due to the high-temperature atmosphere and materials involved in fabrication, it is difficult to observe and even harder to measure *in situ* during the printing process. Only after a part is printed it can be properly analyzed, but the result is a product of the compound behaviors of both the machine and the material itself (Fig. 1).

With special sensitivity to glass behavior, significant importance was assigned to engineering the structural, mechanical, and thermal performance of the machine to improve its control and repeatability, such that unexpected outputs could be attributed to inherent material properties of the glass rather than the machine. As an example of this confounding nature, a product from G3DP had noticeable deviations from the intended tool path at inflection points along its curves, but it was difficult to determine what had caused them (Fig. 2). The fundamental question was whether the deviations occurred as a result of aberrant behavior of the machine or the behavior of the glass.

Platform specification

To evaluate the transition from a prototype system to the industrial system described here, some key performance metrics are provided as a means of examining the improvements that were implemented. These metrics will be contextualized with respect to the goals outlined above, and then additional details on the system will be provided (Table 1).

The first key metric of comparison is scale. An increase in each of the principle axes of the system resulted in a near doubling of the size of the objects that could be fabricated. The mass of the glass reservoir saw an even greater increase, with the ratio of reservoir to print volume rising from 5% to 30% and eliminating the need to refill the reservoir during prints. From an absolute standpoint, this represented an increase in available material by a factor of 12.

The second key metric of comparison is speed. With a minor increase in nozzle size, layer height, and feed rate, the compound effect was a more than doubling in printing rate, making this platform one of the fastest globally, independent of material.[16]

The third and fourth key metrics of repeatability and reliability are harder to compare quantitatively with the previous version. Instead, absolute metrics are presented here to show a definitive result for future comparison. Testing of the G3DP2 system indicates the ability to hold positional accuracy to finer than 1 mm and produce a set of circular products that are within 1 mm of the predicted dimensions. In addition, the new static architecture introduced thermal and mechanical systems that could operate for months at a time without the daily adjustments required by G3DP. Current limitations

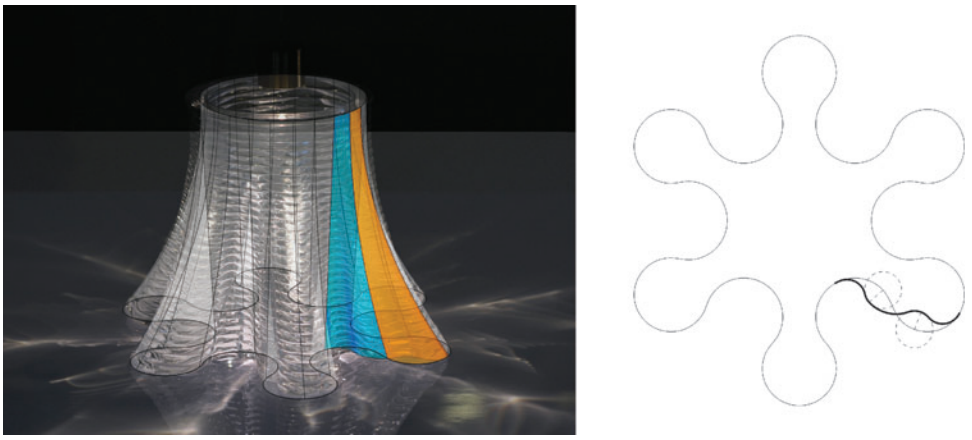

FIG. 2. *Left*: part produced on G3DPwith unexplained deviations from the intended CAD, *orange* highlight indicates convex CAD surface, *blue* indicates concave CAD surface. *Right*: plan view of path of base layer, *bold line* shows deviation from intended profile, *dotted lines* indicate aberrant generated curvatures.

Table 1. Comparison Between the First and Second Generation of the Printer Highlighting Key Metrics

	Unit	G3DP	G3DP2	Change, %
Platform				
X-axis	mm	250	320	128
Y-axis	mm	250	320	128
Z-axis	mm	300	350	117
Print volume	cm^3	18,750	35,840	191
Reservoir size	kg	2.1	25.5	1214
Material ratio	%	4.6	29.0	624
Process				
Nozzle size	mm	10.0	11.5	115
Feed rate	mm/s	6.1	10.0	164
Bead height	mm	4.5	5.0	111
Bead width	mm	9.5	12.0	126
Bead area	mm^2	40	57	145
Print rate	mm^3/s	240	570	238
Flow rate	kg/h	2.2	5.2	234

Absolute values as well as the relative change are included.

in nozzle joinery dictate 2–3 week print campaigns, and ongoing research aims to further extend.

Platform architecture

The G3DP2 platform is a modular system of two-part vertical assembly: the upper thermal and the lower motion control systems are integrated with a separate control station to enable concurrent development and independent system calibration to make future upgrades efficient (Fig. 3).

The thermal control module is an assembly of three independent heating systems that are digitally integrated with a centralized control system to provide a continuous temperature profile across the glass transition temperature from melting to annealing.

The motion control module is the motion control system, a set of linear actuators along X, Y, and Z axes, and an additional A-axis rotary table with an infinite rotation capability about the Z-axis to provide a fourth degree of freedom.

The control station is comprised of two independent sets of power electronics and microcontrollers for the thermal control modules and motion control modules. These modules provide a unified access point and control interface to the thermokinematic control system of the G3DP2 (Fig. 4).

Platform engineering: thermal control

The thermal control module of G3DP2 is a vertical assembly of the following three subsystems: the Material Reservoir, the Nozzle Control, and the Build Chamber. Total power consumption of the thermal module is 19 kW at its peak and $\sim$15 kW during the normal printing cycle.

The Material Reservoir subsystem was designed in collaboration with Skutt, Inc. (Seattle, WA) and Engineered Ceramics (Gilberts, IL). It consists of a custom-designed cast alumina crucible and a resistive wire-based electrical kiln. The kiln supplies 6.5 kW and operates at 1090°C during printing. The crucible was designed with an opening at the bottom and stepped groove in which to mount the nozzle. The kiln is equipped with two type-S thermocouples, and the temperature of the Material Reservoir is managed through the control station.

The Nozzle Control subsystem was designed in collaboration with Deltech, Inc. (Denver, CO) and Smart Ceramics, Inc.

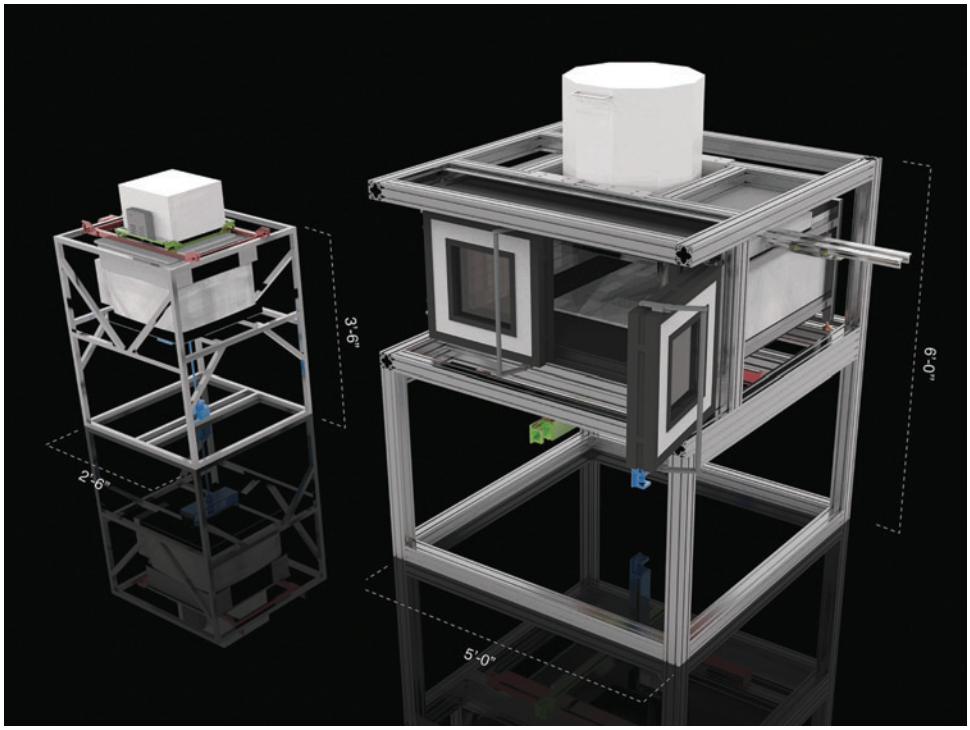

FIG. 3. The two platforms and dimensions of G3DP on the *left*, and G3DP2 on the *right*.

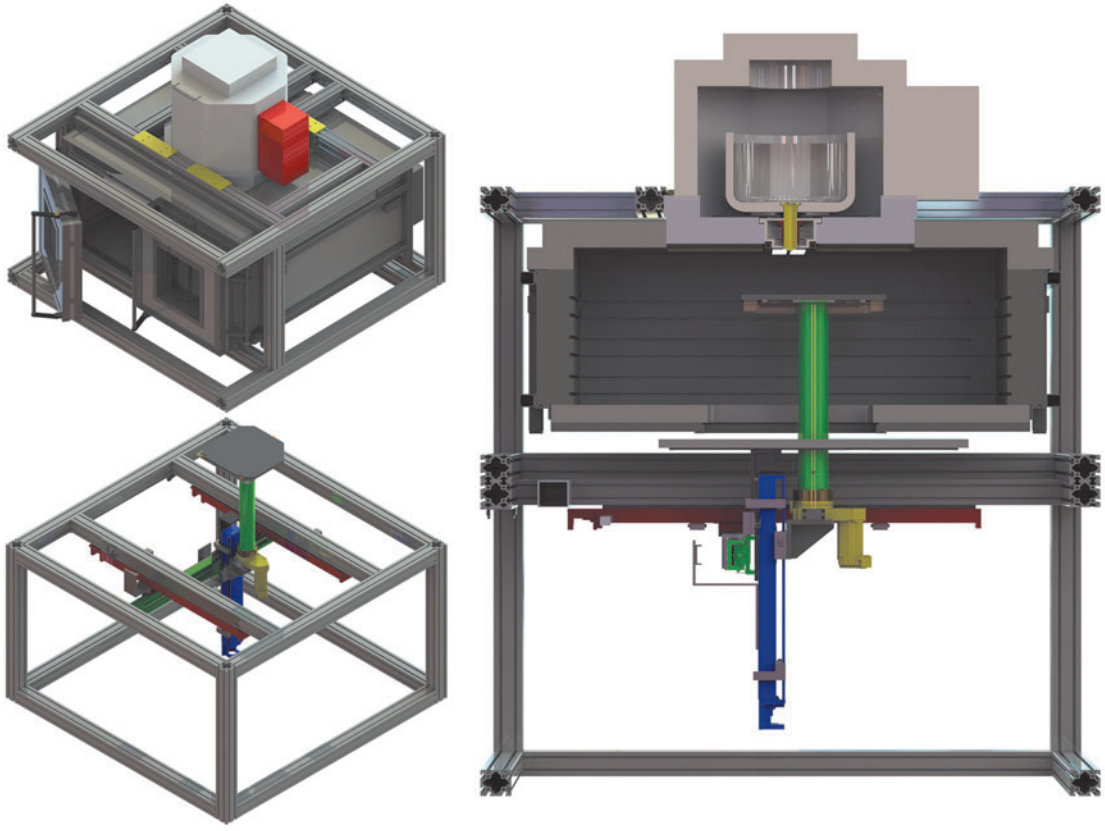

FIG. 4. *Left*: an exploded view of the upper thermal module and the lower motion control module. *Right*: a cross-section of the entire system that reveals the interior detail.

(Woburn, MA). It is located below the Material Reservoir, and consists of a custom-machined alumina nozzle and two-part thermal control mechanisms.

The nozzle acts as an interface between the thermal and mechanical systems of the printer. Molten glass is highly viscous and easily adheres to the bottom exterior face of the ceramic nozzle. This phenomenon, called wetting, became problematic during the previous research phase. Especially when this wetting took place asymmetrically with respect to its central axis, the nozzle applied uneven shear force to the molten glass based on its relative orientation to the direction of deposition, which subsequently distorted the cross-sectional profile and width of the glass filament. The development of G3DP2 focused on managing and mitigating this asymmetric wetting and its effect on print fidelity. To decrease the impact of wetting, the geometry of nozzle tip angle was increased from 30° to 45° to reduce the contact surface area with the molten glass. The nozzle was machined from a solid alumina at the MIT Central Machine Shop (Cambridge, MA) and assembled with the crucible in the Material Reservoir using silica-based refractory cement.

Nozzle body temperature is controlled by a custom-designed resistive wire heating system wrapped around a silicon carbide tubular mandrel. Temperature is controlled by a pair of type-S thermocouples. These components are housed in a structural grade refractory (Smart Ceramics SG-70) forming the nozzle kiln, which supplies 600 W and operates at 800°C during printing.

Nozzle tip temperature is controlled by propane combustion or the application of compressed air through the nozzle gas manifold. The manifold is mounted at the bottom face of the nozzle kiln, concentric to the central axis of the nozzle. Used in conjunction with the nozzle kiln, digital control of the flow initialization and termination process is achieved. Gas is turned on with a digital igniter when used as the burner and is turned off when used as the cooler. Its concentric design allows even distribution of air pressure and thermal stress around the nozzle to prevent asymmetric smearing of the nozzle with directional airflow.

The Build Chamber subsystem was designed in collaboration with Spiral Arts, Inc. (Seattle, WA), and comprised of an electric kiln with interior volume of D1100 × W1100 × H500 mm, full height double doors in the front, and W400 × D400 mm opening on the bottom. The Build Chamber supplies 12 kW and operates at 480°C during printing. It provides dual type-K thermocouples for redundant temperature measurement. The pair of front doors is furnished with double pane Neoceram—a low CTE heat-resistant ceramic—windows and allows process monitoring while maintaining the thermal profile inside. The bottom opening allows the print bed support tube to travel across the entire print size. This opening is sealed by a thermal insulation shield made of a 13 mm thick Duraboard mounted on an aluminum frame support. The shield assembly is mounted on the Z-axis linear actuator and travels in the XY-plane while allowing the print bed support tube to pass through and rotate around the Z-axis.

The Control Station subsystem was developed in collaboration with Spiral Arts, Inc. The system contains an EZ-Zone® Controller from Watlow (St. Louis, MO) providing a single control interface with full back-end and front-end programming capability across all three heating systems that constitute the thermal control system of G3DP2. Back-end control provides proportional-integral-derivative (PID) temperature controls, power output controls, current monitoring, and safety limit controls with network connectivity. Front-end control is enabled by a custom user interface installed on a touchscreen panel from Watlow. This interface allows process temperature control as well as monitoring of the current temperature across all three thermal systems. Current temperatures, target temperatures, and ramp rates can be specified for each thermal module, connecting each process module to a manufacturing system (Fig. 5).

Platform engineering: motion control

Four-axis CNC structure was designed to meet the target repeatability of ±10% relative to the 10 mm filament size, resulting in the maximum deviation of ±1.0 mm in positioning accuracy under the maximum load criteria based on the combination of the target print mass, cantilever length in Z-axis, lateral acceleration in XY-axes, and rotational acceleration in A-axis. The required flexural and torsional stiffness values of each linear actuator were calculated based on these conditions to ensure the target positional accuracy.

The motion control system of the G3DP2 platform is comprised of a custom-designed four-axis CNC system. XYZ-axes consist of a set of linear actuators (LM Guide Actuator Model KR-46; THK Co., Ltd., Tokyo, Japan), serving as both internal free-spanning structures and motion guide rails for the traveling cart inside. A pair of parallel linear actuators forms the X-axis and provides rigidity to support the rest of the motion axes. Y-axis is supported on both ends by the pair of X-axes, acting as a simple free-spanning beam. Z-axis is mounted on Y-axis, acting as a cantilever beam. A-axis, the fourth axis, providing rotational motion around the Z-axis, is made of a precision rotary table (ServoBelt Rotary Stage SBR-50-31; Bell-Everman, Inc., Goleta, CA). The print bed is mounted onto this rotary table with an extension tube forming a rigid connection between the bottom of the support tube and the rotary table. This support tube serves as a thermal break together with an insulation shield panel at the interface between the build chamber and the motion control module.

Four-axis motion control was developed to provide control over the orientation of the print nozzle and the relative direction of the deposition with respect to the trajectory of the

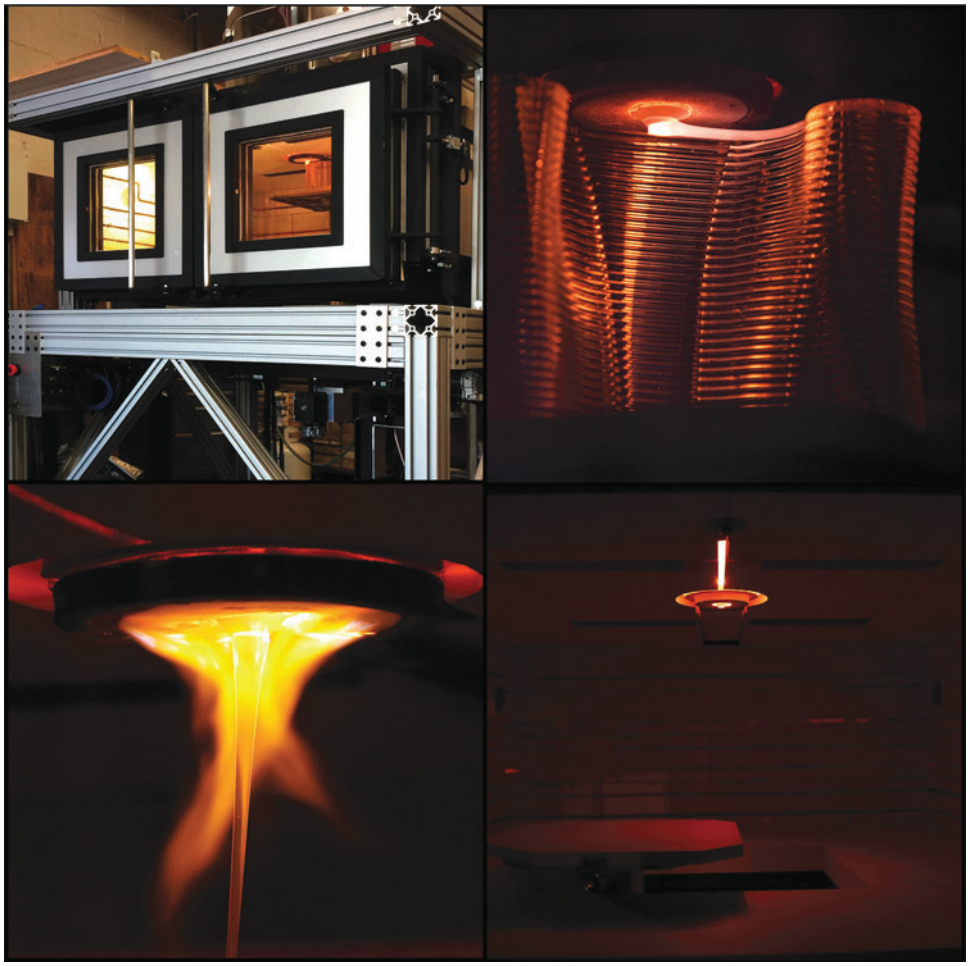

FIG. 5. *Top left*: exterior and interior. *Top right*: G3DP2 platform during the deposition of molten glass. *Bottom left*: nozzle control module gas manifold during heating. *Bottom right*: build chamber during idling before printing is initiated.

print path. It was further expected to address asymmetric wetting of the nozzle and expand the capability of the platform by exploring nozzles with noncircular orifice profiles such as rectangles or nozzles with multiple orifices to enable simultaneous deposition of different glass compositions. Finally, it has the capability to deposit glass of varying thickness as a calligrapher does with pen and ink.

To implement four-axis motion control for the print bed with the stationary nozzle architecture, algorithms were developed to translate input path geometry to required compound motion. A sequence of 3D coordinates (X, Y, and Z) and individual feed rates F1 were assigned to each coordinate, then transformed into four-dimensional coordinates (X, Y, Z, and A) and corresponding feed rates F2 for four-axis CNC motion.

Control and actuators. Motion of all four axes is powered by high torque servomotors (ClearPath SDSK-2341S-RLN; Teknic, Inc., Victor, NY) with integrated encoders that have position and torque feedback loop capability. G3DP2 makes use of the position encoders to attain closed-loop accountability, marking a significant improvement over the open-loop stepper motor motion system of the G3DP platform.

Integration of four-axis motion control is enabled by an open-source CNC controller (TinyG CNC Controller; Synthetos, LLC, Brookeville, MD). Its multiaxis motion control capacity with the open-source architecture enables the ground-up development of custom algorithms for the fourth axis rotational motion and its integration with the three-axis motion control system.

Software. Custom motion control software that executes G-Code commands was developed for the TinyG workspace in Chilipeppr, an open-source JavaScript-based hardware control interface software. It communicates with the TinyG through Serial Port JSON Server to establish the close-loop feedback between the servomotors and the digital interface.

Feedback. To enable automated responses to failure conditions, a bridge was created to communicate high-level feedback from the motors back to the server, which in turn notifies the user interface (UI) and commands the motion controller appropriately. For example, upon failure of the X-axis, an automatic lowering of the Z-axis could prevent damage to the nozzle. Notifying the operator of error reduces waste and helps prevent unnecessary damage.

Accuracy of motion. To evaluate the process fidelity and repeatability of this four-axis motion control, preliminary tests were conducted at room temperature. A pair of pens was used in place of the molten glass to record the system motion. The ceramic nozzle was replaced with two pens fixed side by side, constraining their rotational motion and position to that of the machine. The test was conducted to draw a constant radius two-dimensional curve forming a three-lobe profile by turning on and off the fourth axis rotation, as shown in Figure 6.

First, three-axis positioning accuracy was evaluated with a single pen, making repetitive motions and measuring sample points to ensure basic machine tolerance. Results found the positioning tolerance to be <1 mm. The next series of tests

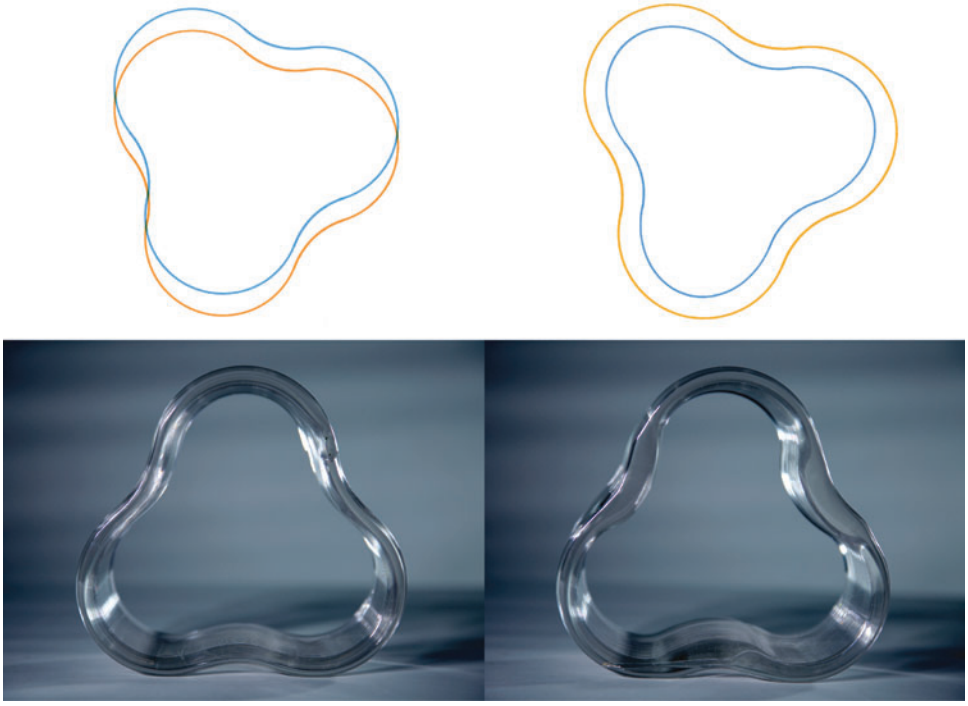

FIG. 6. *Top right*: scan of three-axis pen test. *Left*: scan of four-axis pen test. Nozzle replaced by *blue* and *orange* pens capturing relative orientation between nozzle and build plate during motion. *Bottom left*: test of extrusion with three-axis motion control showing constant wall thickness. *Bottom right*: test of extrusion with four-axis motion showing increased wall thickness at inflection points as a result of jerk-limited accelerations.

were conducted by printing molten glass at temperature. By measuring the system repeatability across 10 cylinders of D200 × H200 mm, positional accuracy was found to be very stable. Average outer diameter was 197.3 mm, or a difference of 2.7 mm (1.4%) compared with the target value of 200 mm, which can primarily be attributed to shrinkage due to thermal expansion. Importantly, when we compare the mean diameter between samples, a maximum range of 0.7 mm (0.3%) with a standard deviation of 0.5 mm (0.3%) was found. These results demonstrate a highly repeatable process at elevated temperature.

Next, the effects of four-axis motion were explored. The results show unexpected changes in wall thickness at every inflection point of the geometry. This effect was more substantial in the four-axis print than in the three-axis print. The increase in wall thickness at the concave sections of the four-axis product is likely a result of acceleration management of the CNC module. To minimize system vibration, the motion system was designed to be jerk limited, where jerk is the second derivative of the velocity with respect to time. The jerk limit slowed acceleration and created a delay in rotational velocity at every inflection point, and thus a decrease in feed rate. This change in feed rate caused inconsistent deposition rates and thus, incorrect wall thickness in parts. Additional development work has already been initiated to optimize acceleration control on the fourth axis. In this article, the products described were printed with three-axis motion.

Platform control

Nozzle flow rate. Following the success of gravity-based flow control achieved with the G3DP platform, the G3DP2 platform employs the same methodology. The flow rate is a function of nozzle resistivity, which is driven by its internal dimensions, and the pressure head of molten glass in the crucible, driven by its height (Fig. 7).[20]

Improved insulation between the Material Reservoir and Build Chamber unfortunately necessitated an increase in nozzle length. To offset the corresponding increase in resistance due to length, the diameters were also increased, providing a modest 17% reduction of nozzle resistance. In combination with a doubling of head pressure, flow rate was more than doubled. Results of this analysis were later confirmed to be very close to the observed behavior.

Flow rate calculation. The flow resistance $\mathcal{R}$ of the crucible–nozzle assembly in the G3DP2 platform is estimated based on the Hagen–Poiseuille equation. $\mathcal{R}$ is a function of the length L and the diameter D of each section of the crucible–nozzle assembly. Here, the change in R is directly proportional to the change in L and inversely proportional to the fourth power of the change in D. Therefore, the smaller the diameter of the tube, the greater the influence of its change on the flow resistance.

$$\mathcal{R} = \frac{8\eta L}{\pi (D/2)^4}. \tag{1}$$

The head pressure P is the pressure difference between the top of the molten glass in the crucible and the bottom of the nozzle. It is a function of the glass density ρ and gravity g, and linearly dependent on the difference in the height H, such that

$$P = \rho g H. \tag{2}$$

The volumetric flow rate Q (m^3/s) of the G3DP2 platform is determined based on the head pressure P (N/m^2) and the flow resistance $\mathcal{R}$ [$N/m^2/(m^3/s)$], such that

$$Q = \frac{P}{\mathcal{R}}. \tag{3}$$

Platform operation

The platform operation of the printer can be divided into the following three phases: preprinting, printing, and

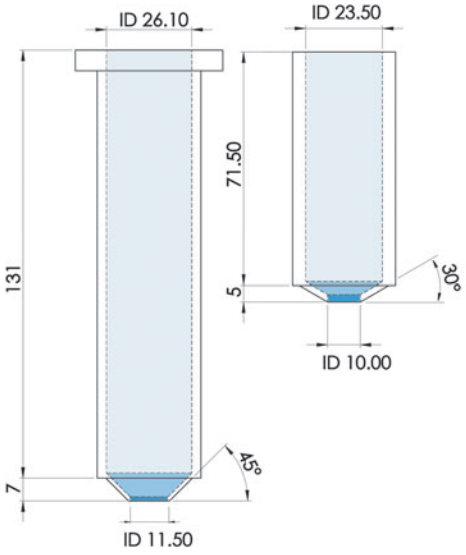

Region	G3DP	G3DP2	Change
Section1 Resistance	6.3E+09	7.6E+09	121%
Section2 Resistance	2.8E+09	2.7E+09	97%
Section3 Resistance	6.1E+09	2.3E+09	38%
Resistance Total	1.5E+10	1.3E+10	83%

	G3DP	G3DP2	Change
Pressure	3.6E+03	7.1E+03	198%
Flow Rate Predicted	2.4E+02	5.6E+02	238%

FIG. 7. *Left*: dimensions of G3DP and G3DP2 nozzles. *Right*: effects on nozzle resistance of geometric changes are shown.

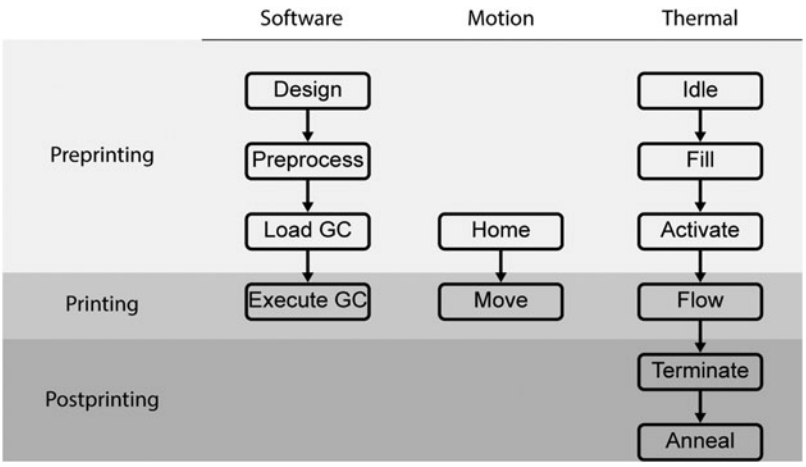

FIG. 8. Print phases and the corresponding actions of software, motion control and thermal control are shown.

postprinting. In this section, key process steps are examined in software, motion control, and thermal control (Fig. 8).

Preprinting. During the preprocessing stage, a series of operations are prepared in parallel to begin fabrication. In software, design of the desired object is processed with a C# script to form a single continuous path. Then, this print path is converted from geometry into a series of actions for each motor to execute in the form of G-Code. The Chilipeppr control interface loads the file and compiles commands to the TinyG and ultimately, to the motors that command the printer to trace out the desired path.

In hardware, the platform is readied. The motion system is homed to re-establish the origin of the system. The thermal control module is kept in an idling mode. In this state, the Nozzle Control subsystem is set at a reduced temperature of 800°C, maintaining an environment in which glass is unable to flow through the nozzle. The Glass Reservoir and Build Chamber are both kept at the standard operating temperature.

The printer is filled with build material for the upcoming print. While idling, the printer can be refilled with either molten glass or room temperature cullet (preprocessed solid glass pieces that are already melted and conditioned from the constituent raw materials). For expediency of operation, molten glass is typically used. The material is transferred from a large auxiliary furnace using a gather ball, a typical glass-casting tool, to the Material Reservoir.

With all other preprinting steps complete, the thermal module of the system can now be readied for flow. This is achieved by increasing the temperature set point of the nozzle kiln from 800°C to 915°C. In conjunction, the nozzle gas manifold is activated to heat the nozzle tip. The combined effect of these thermal changes initiates the flow of molten glass. After glass begins to flow, the burner is extinguished, allowing the nozzle to reach a steady-state flow condition.

Printing. After flow has reached steady state, printing can begin. G-Code is sent from the Chilipeppr interface to the TinyG motion controller, and the build plate begins to move to initialize printing.

Postprinting. Upon completion of the G-Code file, the printed object is subjected to a thermal soak at 525°C for ~5 min, providing a temperature buffer while it is transported to an external annealing oven. While the Build Chamber in the G3DP2 platform is capable of annealing each print, an external oven is utilized to facilitate the production cycle.

Finally, the flow of glass is terminated by lowering the set point of the Nozzle Control subsystem back to the idle temperature of 800°C and by activating the compressed air sent through the ring manifold.

The Product Space

Process to product

One of the key objectives in this research was to develop a new AM technology for glass capable of addressing the scalability in both quality and quantity required to transition from a proof of concept to a full-scale industrial manufacturing platform. Production accountability is of specific importance to industrial glass due to the physical nature of the material. While soda-lime glass has a theoretical strength of ~10,000 MPa, real-world microscopic flaws within the material restrict nominal tensile strength to a range of 40–80 MPa.[19] Additional surface flaws created by various manufacturing processes, along with the brittle nature of glass, result in extremely high safety factors in structural applications, leaving designers and engineers with a maximum allowable strength of just 10 MPa.[21] Therefore, this research works toward a high-fidelity manufacturing platform capable of translating design input into glass products with known tolerances and reliable performance through process understanding and mechanical characterization. This enables novel glass designs that take advantage of the optical transparency and mechanical strength of the material, culminating in the design and installation of a first expression of the technology at the architectural scale—a public installation of a set of 3-m-tall freestanding 3D-printed glass columns.

The following section presents the design space and associated design methodologies developed along with the G3DP2 platform, specifically relating to material behavior and machine engineering. Also presented are methods for characterization and validation of products and components, the results of which serve as a performance evaluation for this new manufacturing platform.

Product design space

Extreme operating temperatures and high viscosity of glass create a challenge in any manufacturing process, and must be accounted for dynamically in a 3D printing context. The glass filament cools relatively slowly and maintains a low enough viscosity that resulting dynamic shear forces may alter the geometry of previously deposited glass during printing. Sensitivity to this material–process interaction is critical, and can manifest as a nonlinear response of molten glass, including curvature and rate of change. To limit this effect, print curvature must be an explicitly controlled variable in the design space.

Traditional 3D printing processes accept input geometry as 3D surfaces. The geometry is sliced horizontally, and its boundaries are implicitly translated into filament deposition paths acceptable to the constraints of the machine, inevitably leading to filament-scale deviations from design input. G3DP2 utilizes a molten glass filament with a diameter of 10 mm, an order of magnitude larger than most of the synthetic filaments used in the commercially available extrusion-based 3D printers, and consequently the subtle deviations in position and curvature at filament scale cause substantial effect on output geometry.

To establish the process fidelity at this filament scale and control the curvature-dependent material behavior, the requirements for the design process were re-evaluated in parallel to the system re-engineering. As a result, a suite of computational algorithms was developed to establish a parametric design space for glass products, where product morphologies are explicitly managed at the design input level, by the control of curvatures and their rates of change in 3D space, affording a lossless input to output design flow. This parametric framework enables a multivariable cross-domain design space, where the geometric variables of the design can be directly linked to external variables such as the feed rate in the machine domain, focal point of incoming lights in optics domain, and section modulus and other properties in the structural domain.

From the design of parametric geometries to preparation of executable G-Code file for the CNC platform, the connecting computational process was developed as an integrated series of computational algorithms written in C# and implemented with a 3D CAD software and programming interface (Rhinoceros 5.0 and Grasshopper 1.0; Robert McNeel and Associates, Seattle, WA). Curvature-based parametric design space was explored. The algorithm takes three arguments as input variables: a floating-point variable R1 denoting the radius of a circumscribing circle that defines the exterior boundary of the output geometry, a floating-point variable R2 defining the radii of a network arcs and bitangent arcs, and an integer variable *N* defining the number of arcs within the single closed profile curve.

Here, various geometric configurations in two-dimensional space were explored morphologically in continuous domains by incrementally changing each input variable. A series of case studies were conducted to evaluate the influence of different curvatures on printed glass output. Five objects were printed with constant R1 value of 150 mm, incremental R2 values of 150, 60, 30, 20, and 15 mm, and *N* values of 1, 3, 6, 12, and 24, respectively, denoting the number of lobes formed per object (Fig. 9).

Next, 3D morphologies were explored by assigning a number of instances in vertical axis corresponding to the layer count LC, an offset height between each instance corresponding to the layer height LH, and a rate of change for each radius ΔR1 and ΔR2.

By taking this curvature-dependent and process-informed approach, we were able to expand the preliminary design space where glass products and architectural designs began to form within the constraints of the newly formed machine space. The components printed through this approach were repeatable in fabrication and without deviations from expected tool path such as those observed on the previous generation platform.

Mechanical characterization

Throughout the engineering phase of the new manufacturing platform and design phase of the new glass products, a series of geometric and mechanical characterizations were conducted to evaluate the dimensional tolerance and repeatability as well as the mechanical responses of the 3D-printed glass products under various loading conditions. These findings guided the product specifications for the new products and served to evaluate the process fidelity of the new platform. The appropriate safety factors for the design and engineering of the 3D-printed glass structures were derived from these results.

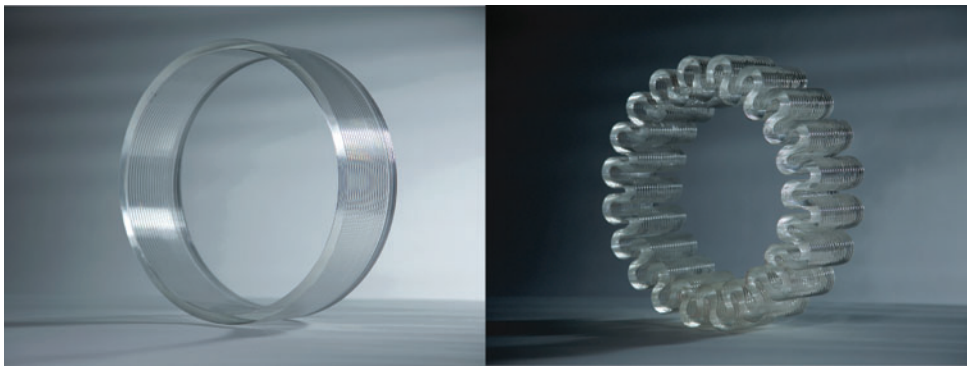

FIG. 9. *Left*: 3D-printed glass object with R1 = 150, R2 = 150, *N* = 1. *Right*: 3D-printed glass object with R1 = 150, R2 = 15, *N* = 24.

Table 2. Geometric Data for Single-Point Bending Test Samples

Treatment	*Sample*	*ID, mm*	H, *mm*	*IT, mm*	Z, mm^3	I, mm^4
Annealed	1	285.9	98.2	8.8	1300	5600
Annealed	2	284.5	98.0	9.4	1400	6800
Tempered	3	286.6	98.0	9.0	1300	5900
Tempered	4	285.6	97.8	9.4	1400	6700
	Range Δ	2.1	0.4	0.6	100	1200
	%	0.74	0.4	7	7	19

For the initial geometric and mechanical characterizations, eight standard cylindrical samples of 3D-printed glass products (R150 mm, H100 mm) were tested. All samples were fully annealed before the characterizations. Of the eight samples, four were chemically tempered (noted hereafter as tempered), and the other four were left as nontempered (noted hereafter as annealed). Two samples of each were used in single-point bending tests on the major axis along the grains of layers at full scale. The other two samples of each were sliced in segments for use in three-point bending tests on the minor axis.

Major axis single-point bending tests. Inside diameter ID, cylinder height H, and interior wall thickness IT, defined as the minimum width of the wall occurring between layers, were measured at each quadrant along the circumference of each sample digital caliper. The average values and range of values from each sample were calculated from the measurements. The following table presents a summary of the dimensional properties and measured tolerances along with the resulting section properties and their expected tolerances, where the section modulus Z and the area moment of inertia I determine the structural performance of each product. Given the quadratic and cubic order relationship to the linear dimensions, the expected ranges of section properties and structural performances of products are far more sensitive than the dimensional variations governed by the manufacturing processes (Table 2).

Mechanical characterizations were carried out in the material research laboratory at the Simpson Gumperz & Heger, Inc. (Waltham, MA). MTS-30G Uniaxial Load Frame with 30 kN load cell was used for the major axis single-point bending tests on the full-scale cylindrical prints of D300×H100. Based on the peak load F and the corresponding peak displacement δ, along with the estimated Z and I, the peak stress σ and the elastic modulus E for each sample were calculated using Castigliano's theorem on bending dominant systems. Considering the single-point load P applied to a thin curved beam with radius R, the maximum bending moment M and the maximum displacement δ take place at the top quadrant of the structure, and their corresponding values were calculated accordingly.

$$\delta = \frac{FR^3}{EI}\left(\frac{\pi}{4} - \frac{2}{\pi}\right) \tag{4}$$

$$\sigma = \frac{M}{Z} = \frac{FR}{\pi Z}. \tag{5}$$

The following table provides the summary of the major axis bending tests. F and δ were measured peak values from each sample, whereas σ and E were calculated values. Expected ranges presented for σ and E based on the corresponding dimensional variability calculated previously for Z and I (Table 3 and Fig. 10).

Minor axis three-point bending tests. Minor axis three-point bending tests were conducted to evaluate potential anisotropic responses of the 3D-printed glass products due to their corrugated textures on exterior and interior surfaces. Two annealed and two tempered cylindrical samples were sliced across the grains of layers into rectilinear bars of ~13.0 mm width. MTS-30G Uniaxial Load Frame with 30 kN load cell was used for the test. The following table presents the average dimensional properties, including test span L, measured from each sample along with the resulting section properties (Table 4).

Peak load P was directly measured from the tests. Corresponding displacement δ was adjusted based on the offset value determined by the intersection between the slope of the linear elastic region of the load-displacement curve and the

Table 3. Load Test Results and Corresponding Calculations of Internal Stress and Elastic Modulus Are Reported

Treatment	*Sample*	F, *N*	*δ, mm*	*σ, MPa*	E, *GPa*
Annealed	1	1240	1.7	47	65
Annealed	2	1690	1.7	56	74
Tempered	3	1060	1.4	39	65
Tempered	4	3050	3.3	100	71
Annealed	Range Δ	450	0.0	9.0	9.0
	%	30.7	0	17	13
Tempered	Range Δ	1990	1.9	61	6.0
	%	96.8	81	88	8.8

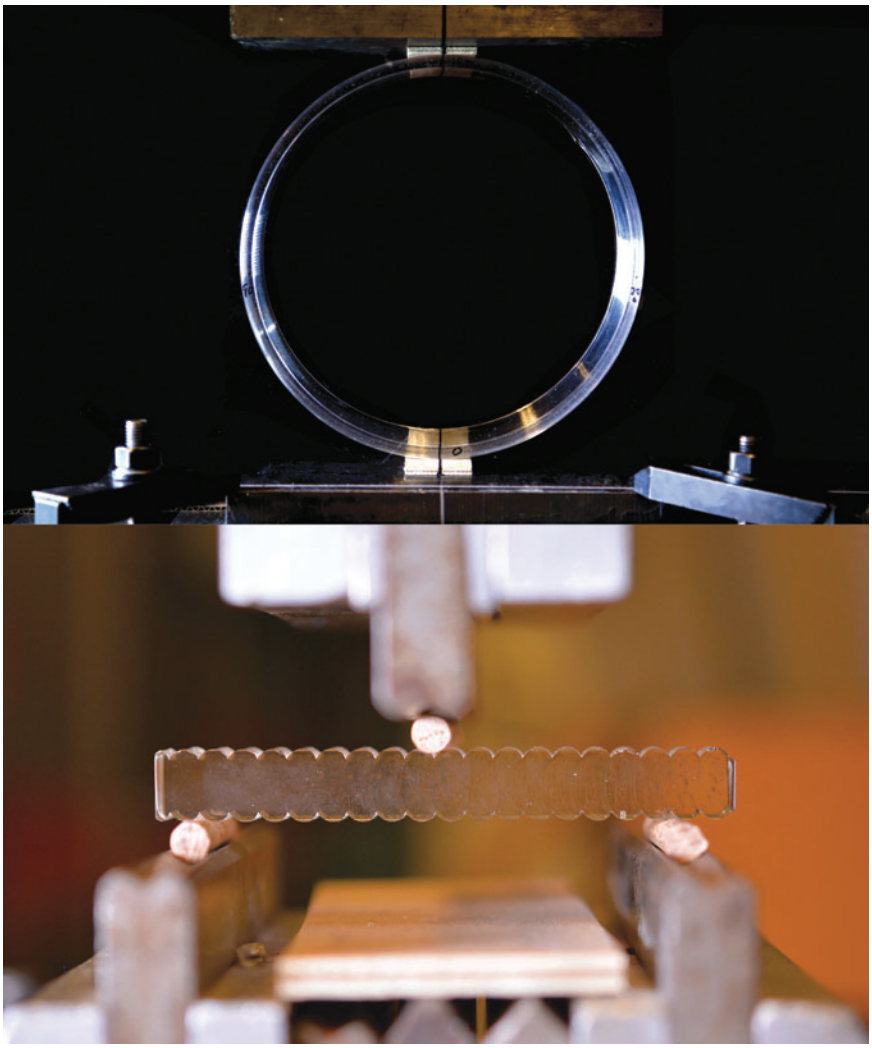

FIG. 10. *Top*: single-point bending test of 3D-printed glass cylinders shown during structural failure. *Bottom*: sample during minor axis three-point bending test.

horizontal axis of the displacement. Based on the Euler–Bernoulli beam theory on a simple beam structure, the maximum bending moment M, ultimate stress σ, and elastic modulus E were calculated using the test results F, δ, and the section properties Z and I that were estimated based on the measured dimensional properties of each sample.

$$\delta = \frac{FL^3}{48EI} \tag{6}$$

$$\sigma = \frac{M}{Z} = \frac{FL}{4Z} \tag{7}$$

The next table presents the results from the minor axis three-point bending tests on the rectilinear bar samples (Table 5).

Discussion

While the small sample size of this data set does not yet provide comprehensive material properties of glass, it does

TABLE 4. GEOMETRIC DATA FOR SINGLE-POINT BENDING TEST SAMPLES

Treatment	*Sample*	L, *mm*	*W, mm*	*IT, mm*	*Z, mm*^{3}	*I, mm*^{4}
Annealed	Avg	69.9	13.1	8.5	160	660
	Range Δ		1.2	0.3	7.6	33
	%		9.1	3.7	4.9	5.1
Tempered	Avg	79.4	13.7	9.0	180	830
	Range Δ		1.2	0.6	28	170
	%		9.1	7	15	21

Table 5. Test Results of Minor Axis Three-Point Bending with Maximum Load *P*, Displacement Δ and the Calculated Moment *M*, Stress Σ, and Elastic Modulus *E*

Treatment	*Sample*	F, *N*	*δ, mm*	*σ, MPa*	E, *GPa*
Annealed	Avg	360	0.05	41	71
	Range Δ	260	0.03	31	18
	%	71	56	76	25
Tempered	Avg	380	0.07	41	67
	Range Δ	350	0.02	34	58
	%	93	35	83	86

provide a basis on which to design and execute glass products. In addition, it shows initial agreement within a range of expected values.

Average tensile yield strengths for the annealed samples were 51 MPa in major axis single-point bending tests and 41 MPa in minor axis three-point bending tests. These values are in line with commonly accepted values for soda-lime glass mechanical strength.

Tempered samples recorded strengths at the extremes of the range. The increased range of results and lower minimum strength led us to focus initially on annealed glass. Further studies are warranted to better understand the source of this variability and the potential increase in strength that certain samples exhibit.

The strength of the structural design of the columns adopts a high safety factor of 10, combining a typical building safety factor with an additional material safety factor to account for the uncertainty created by the wide range of results and small sample size of the tests. Maximum design strength of the 3D-printed glass products was derived as 4.1 MPa, and served as an upper bound for the design and engineering of the three unique glass column structures discussed in the next section.

Public installation of the glass structures

Using the G3DP2 technology and a series of preliminary geometric and mechanical characterizations of its products, a set of 3-m-tall structural glass columns were produced for an architectural installation for the Lexus ''Yet'' exhibition during Milan Design Week 2017. In the new glass design space and material-informed parametric framework, the columns were designed with curvature-dependent methods for geometric morphology, which provided repeatable results in the preliminary design evaluations presented earlier. This repeatability and predictability of manufacturing tolerances strongly inform the derivation of safety and performance factors and the resulting opportunities for design.

The glass columns were structurally optimized within this predictable domain for performance as freestanding cantilever columns with continuous cross-sectional morphology along their height. The cross-sectional profiles at any are defined by a single constant curvature composed of a network of constant radius arcs and bitangent arcs. Along the vertical axis of the columns, that radius undergoes incremental linear change to smoothly transition its morphology in both lateral and longitudinal directions, resulting in bifurcating lobe structures. The continuity of morphology prevented stress concentrations at any local point across the structures. The bifurcation relates structural performance to cross-sectional moment of inertia, with the greatest moment occurring at the point of greatest bending load and continuously decreasing until the point of least load.

Individual columns were constructed from sets of 15 unique printed glass components that were assembled vertically with thin silicone film joinery and steel post-tensioning systems to ensure vertical stability. Each column contained a mobile LED light module set on a linear motion system, with illumination controlled by the intersection of the moving light rays and the continuous morphology of the glass structure. This created a dynamic display of large-scale caustic patterns, expressing the incredible potential of glass

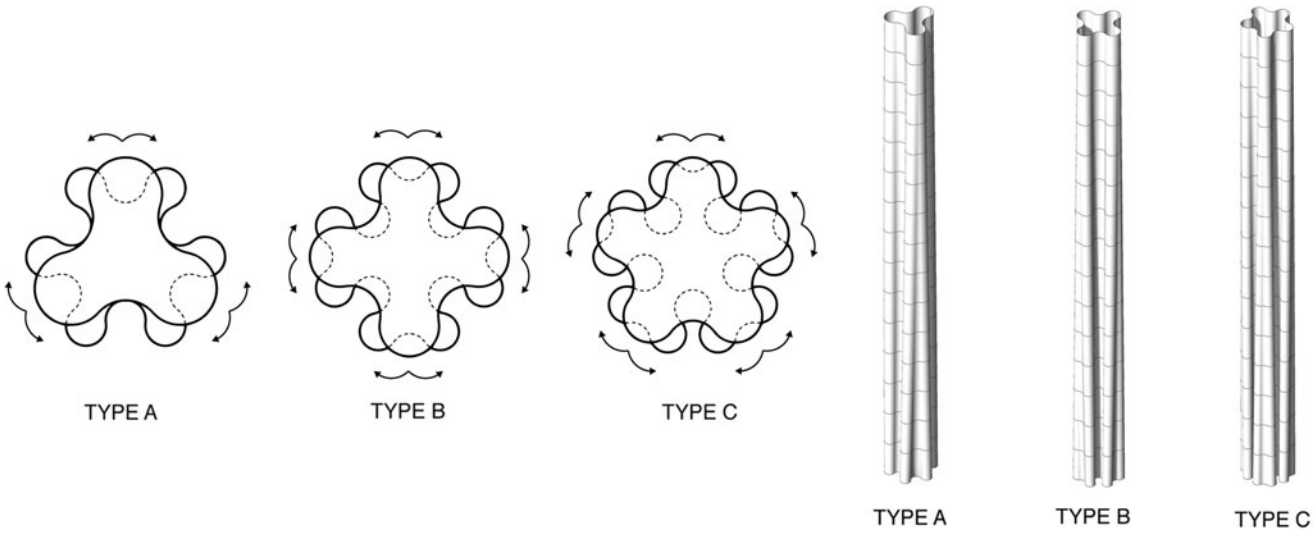

FIG. 11. *Left*: cross-section diagram of the glass columns. *Right*: isometric view of the three instantiations of the glass columns.

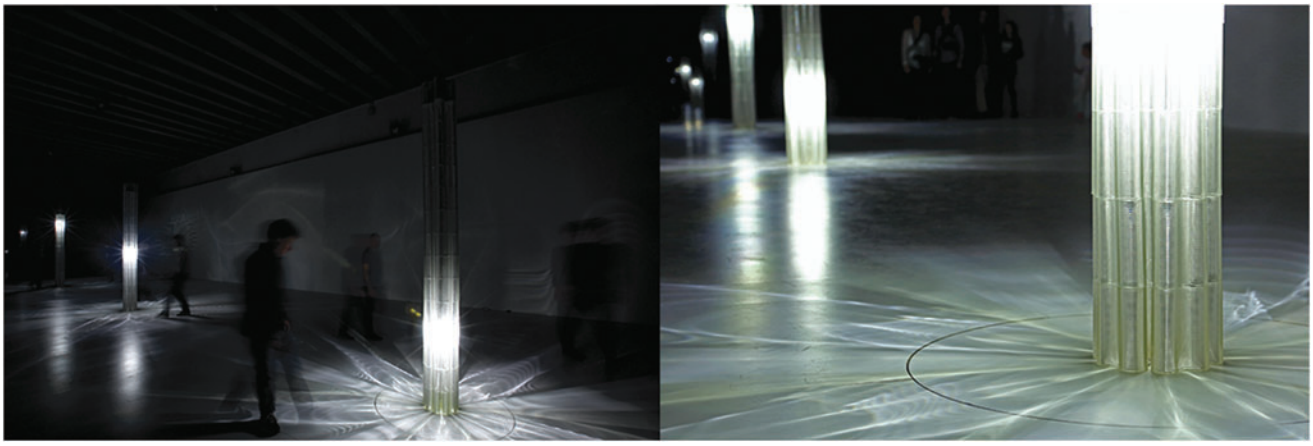

FIG. 12. *Left*: 3D-printed glass columns displayed during Milan Design Week 2017. *Right*: close-up view of one of the glass columns and the caustics projected on the floor.

structures and illumination systems at an architectural scale (Figs. 11 and 12).

Conclusion

From the development of a new manufacturing technology to the deployment of novel products, which demonstrate its capability through the construction of the large-scale printed glass structures, this article presents a promising application of AM technology for glass at industrial-scale production; a technology that builds upon the concept previously introduced by the G3DP platform and exhibits significant improvement of the fidelity and reliability, while achieving faster production speed and volume, all critical to its industrialization.

Glass is brittle, susceptive to stress concentration, and often considered to be fragile and even avoided as a material for structural applications. AM is undergoing exponential growth in both research and application, yet leaves many questions unanswered when it comes to the structural applications. At the intersection of these challenges, an archetype for building structure—the column—was chosen to set research objectives and requirements for the development of our new platform and as demonstration of the challenges and capabilities.

The installation presented here demonstrates the potential of this AM technology to produce freestanding glass structures for the first time at architectural scale. The set of 3-m-tall glass columns manifests their own structural integrity afforded by the novelty and capability of the new manufacturing platform.

In the future, combining the advantages of this AM technology with the multitude of unique material properties of glass such as transparency, strength, and chemical stability, we may start to see new archetypes of multifunctional building blocks. Transparent and hollow-section glass tubes simultaneously act as an heating, ventilation, and air conditioning (HVAC) system, performing as structure and vasculatures at the same time at building scale, through which synthetic and biological mediums circulate and react to incoming sunlight and surrounding temperature, passively regulating the building while illuminating the interior space as if they were a dynamic stained glass—embodying the fundamental shift in the notion of glass in architecture from human centric toward a symbiosis between human, inhuman, and the built environment.

Acknowledgments

We thank Mori Building Co. Ltd. for their initial support and funding for the development and invention of the G3DP2 platform, Lexus Design for their support in producing and hosting the first architectural installation in 3D-printed glass, as well as GETTYLAB for their continued support of research into 3D-printed glass; Andrew Magdanz, Susan Shapiro, Mary Ann Babula, D.J. Benyosef, and Robert Phillips of Almost Perfect Glass for hosting the team and providing invaluable hard work and insights into glass making; Spiral Arts, Inc., Nikon USA, Smart Ceramics, Skutt Kilns, Teknic, Inc., THK, Bell-Everman, Deltech Furnaces, Engineered Ceramics, the MIT Central Machine Shop, and Simpson Gumpertz & Heger for their technical support and collaborative development of the glass printing technology; Front Inc. and Pentagram for additional contributions to the installation La Triennale di Milano for hosting our exhibition; the MIT Media Lab and the MIT Center for Bits and Atoms for use of their facilities; and The Mediated Matter Group for their continuing teamwork and help at every stage of the project.

Authors' Contributions

Design and development of the G3DP2 platform were led and conducted by Chikara Inamura (MIT Media Lab), Daniel Lizardo (MIT Media Lab), Michael Stern (MIT Lincoln Laboratory/MIT Media Lab), Tal Achituv (MIT Media Lab), Peter Houk (MIT Glass Lab), Sadie Whitcher (MIT Glass Lab), Niels LaWhite (MIT Glass Lab), and Professor Neri Oxman (MIT Media Lab). Fabrication and installation of glass columns for Milan Design Week were completed by the platform development team along with Giorgia Franchin (Università degli Studi di Padova), Nassia Inglessis (Royal College of Arts), Tomer Weller (MIT Media Lab), and Owen Trueblood (MIT Media Lab). Image credits go to Paula Aguilera, Jonathan Williams, Andrew Ryan, and The Mediated Matter Group.

Author Disclosure Statement

C.I., M.S., D.L., P.H., and N.O. are listed inventors on patent application US15331898, ''Methods and Apparatus for Additive Manufacturing with Molten Glass.''

References

1. Pratt EE. The Glass Industry: Report on the Cost of Production of Glass in the United States. Washington, DC: Department of Commerce, Bureau of Foreign and Domestic Commerce, 1917.
2. Uusitalo O. Float Glass Innovation in the Flat Glass Industry. Cham, Switzerland: Springer International Publishing, 2014.
3. US Bureau of the Census. Twelfth Census of the United States, Taken in the Year 1900. Population Part I. Volume I. Washington DC: United States Census Office, 1901.
4. Nippon Sheet Glass Co. Ltd. Pilkington and the Flat Glass Industry. In: Glass Industry, 2010. Available at: https://www.pilkington.com/resources/pfgi2010.pdf (last accessed April 18, 2018).
5. United States Census Bureau. Age and sex: 2012–2016 American Community Survey 5-year estimates, 2016. Available at: https://factfinder.census.gov/faces/tableservices/jsf/pages/productview.xhtml?src=CF (last accessed April 18, 2018).
6. British Museum. Collection Online—Window Pane. Available at: www.britishmuseum.org/research/collection_online/collection_object_details.aspx?objectId=466288&partId=1&searchText=roman+window&images=true&pa (last accessed August 1, 2018).
7. Wittel Falk, Wangler T. Science and engineering of glass and natural stone in construction. Available at: www.ifb.ethz.ch/education/msc-courses/msc-science-of-glass-stone-in-construction.html (last accessed January 31, 2018).
8. Statista. Glass industry, 2018. Available at: https://www.statista.com/study/43866/glass-industry (last accessed March 26, 2018).
9. Wohlers T. Wohlers Report 2017. 3D Printing and Additive Manufacturing State of the Industry. In: Wohlers Report 2017. Fort Collins, CO: Wohlers Associates, 2017.
10. The Ex One Company LLC. The New Standard for Manufacturing from ExOne. 2012. Available at: http://prometal.com/sites/default/files/brochures/X1_General_sellSheets.pdf (last accessed January 9, 2015).
11. Marchelli G, Prabhakar R, Storti D, *et al.* The guide to glass 3D printing: Developments, methods, diagnostics and results. Rapid Prototyp J 2011;17:187–194.
12. Kotz F, Arnold K, Bauer W, *et al.* Three-dimensional printing of transparent fused silica glass. Nature 2017;544:337–339.
13. Destino JF, Dudukovic NA, Johnson MA, *et al.* 3D printed optical quality silica and silica–titania glasses from sol–gel feedstocks. Adv Mater Technol 2018;3:1–10.
14. Asiga. The PICO2, 2017. Available at: https://www.asiga.com/products/printers/pico2 (last accessed December 21, 2017).
15. Asiga. Precision on your desktop. 2013. Available at: https://www.asiga.com/media/main/files/printers/Pico Brochure_us_en.pdf (last accessed April 6, 2018).
16. Gutowski T, Jiang S, Cooper D, *et al.* Note on the rate and energy efficiency limits for additive manufacturing. J Ind Ecol 2017;21:S69–S79.
17. Today Prototype. Micron3DP Announces Improved Glass 3D Printer, 2017. Available at: www.prototypetoday.com/micron3dp/micron3dp-announces-improved-glass-3d-printer (last accessed January 1, 2017).
18. 3DPrinting. Micron3DP Completes Installation of Pioneering Glass 3D Printer, Prepares for Beta Release, 2017. Available at: https://3dprint.com/167638/micron3dp-glass-3d-printer-beta (last accessed December 21, 2017).
19. Khorasani N. Design Principles for Glass Used Structurally. Lund, Sweden: Lund University, 2004.
20. Klein J, Stern M, Franchin G, *et al.* Additive manufacturing of optically transparent glass. 3D Print Addit Manuf 2015;2:92–105.
21. Feldmann M, Kasper R, *et al.* Guidance for European Structural Design of Glass Components. Luxembuorg: Publications Office of the European Union, 2014.

Address correspondence to:
Neri Oxman
The Mediated Matter Group
MIT Media Lab
Massachusetts Institute of Technology
Cambridge, MA 02139

E-mail: neri@mit.edu